

# Near-ground ozone source attributions and outflow in central eastern China during MTX2006

J. Li<sup>1,2</sup>, Z. Wang<sup>2</sup>, H. Akimoto<sup>1</sup>, K. Yamaji<sup>1</sup>, M. Takigawa<sup>1</sup>, P. Pochanart<sup>1</sup>, Y. Liu<sup>1</sup>, H. Tanimoto<sup>3</sup>, and Y. Kanaya<sup>1</sup>

<sup>1</sup>Frontier Research Center for Global Change, Japan Agency for Marine-Earth Science and Technology, Japan

<sup>2</sup>State Key Laboratory of Atmospheric Boundary Layer Physics and Atmospheric Chemistry (LAPC), Nansen-Zhu International Research Center (NZC), Institute of Atmospheric Physics, Chinese Academy of Sciences, Beijing, People's Republic of China

<sup>3</sup>National Institute for Environmental Studies, Tsukuba, Japan

Received: 7 April 2008 – Published in Atmos. Chem. Phys. Discuss.: 10 July 2008

Revised: 29 September 2008 – Accepted: 28 October 2008 – Published: 11 December 2008

**Abstract.** A 3-D regional chemical transport model, the Nested Air Quality Prediction Model System (NAQPMS), with an on-line tracer tagging module was used to study the source of the near-ground (<1.5 km above ground level) ozone at Mt. Tai (36.25° N, 117.10° E, 1534 m a.s.l.) in Central Eastern China (CEC) during the Mount Tai eXperiment 2006 (MTX2006). The model reproduced the temporal and spatial variations of near-ground ozone and other pollutants, and it captured highly polluted and clean cases well. The simulated near-ground ozone level over CEC was 60–85 ppbv (parts per billion by volume), which was higher than values in Japan and over the North Pacific (20–50 ppbv). The simulated tagged tracer data indicated that the regional-scale transport of chemically produced ozone over other areas in CEC contributed to the greatest fraction (49%) of the near-ground mean ozone at Mt. Tai in June; in situ photochemistry contributed only 12%. Due to high anthropogenic and biomass burning emissions that occurred in the southern part of the CEC, the contribution to ground ozone levels from this area played the most important role (32.4 ppbv, 37.9% of total ozone) in the monthly mean ozone concentration at Mt. Tai; values reached 59 ppbv (62%) on 6–7 June 2006. The monthly mean horizontal distribution of chemically produced ozone from various ozone production regions indicated that photochemical reactions controlled the spatial distribution of O<sub>3</sub> over CEC. The regional-scale transport of pollutants also played an important role in the spatial and temporal distribution of ozone over CEC. Chemically produced ozone from the southern part of the study region can be transported northeastwardly to the northern rim of CEC; the mean contribution was 5–10 ppbv, and it reached 25 ppbv

during high ozone events. Studies of the outflow of CEC ozone and its precursors, as well as their influences and contributions to the ozone level over adjacent regions/countries, revealed that the contribution of CEC ozone to mean ozone mixing ratios over the Korean Peninsula and Japan was 5–15 ppbv, of which about half was due to the direct transport of ozone from CEC and half was produced locally by ozone precursors transported from CEC.

## 1 Introduction

The importance of tropospheric ozone (O<sub>3</sub>) on air quality, atmospheric chemistry, and climate change has been recognized over the last several decades (Brasseur et al., 1999; IPCC, 2001). In addition to the downward injection of stratospheric ozone, photochemical reactions involving oxides of nitrogen (NO<sub>x</sub> = NO + NO<sub>2</sub>), carbon monoxide (CO), methane (CH<sub>4</sub>), and volatile organic compounds (VOCs) also play key roles in ozone production, especially in industrialized regions (Crutzen et al., 199).

Along with rapid urbanization and industrialization processes, the emissions of O<sub>3</sub> precursors have significantly increased in China; this is in contrast to a significant decrease in Europe and little change in North America and Japan (Naja and Akimoto, 2004; Streets and Waldhoff, 2000). Central Eastern China (CEC, 30° N–40° N, 110° E–130° E) is the biggest emitter of anthropogenic trace gases and aerosols in China (NO<sub>x</sub> emissions reached 3600 Gg/a in 2000, which was 32% of the total emissions in China) (Streets and Waldhoff, 2000). CEC also exhibited a continuous and marked increase in tropospheric NO<sub>2</sub> column densities during the period 1996–2004 (Akimoto et al., 2006; Richter et al., 2005). Consequently, regional-scale high ozone concentrations have



Correspondence to: J. Li  
(lijie8074@jamstec.go.jp)

been recorded near ground in this region in early summer (Ding et al., 2008; Li et al., 2007).

From our observations at three mountain sites (Mt. Tai, Mt. Hua, and Mt. Huang) located in the middle, west, and south of CEC, respectively, the maximum monthly ozone concentration ( $>60$  ppbv) occurred in May–June, with a maximum hourly ozone level  $>150$  ppbv (Pochanart, personal communication; see also Li et al., 2007). Observations at Shangdianzi (a rural site in northern CEC) showed that averaged maximum hourly ozone in June exceeded 120 ppbv (Liu et al., 2006). During a 39-day observation in a rural area located north of Beijing in June–July 2005, Wang et al. (2006a) found that there were 13 days with a 1-hr  $O_3$  mixing ratio that exceeded 120 ppbv, with a maximum level of 286 ppbv, the highest value reported in the literature for China. High ozone levels have been reported frequently at Lin'an, another rural site in southern CEC (Cheung et al., 2001; Wang et al., 2001a; Xu et al., 2008). Gao et al. (2005) reported that the monthly mean ozone concentration in local air masses over CEC was  $>60$  ppbv in July. Modeling studies further support the this data and demonstrate that CEC has the most net chemical production over East Asia in summer (Li et al., 2007; Yamaji et al., 2006; Zhu et al., 2004).

Regional-scale transport of pollutants likely plays an important role in the high  $O_3$  levels that occur over CEC. Satellite-measured tropospheric  $NO_2$  column densities showed an increase of 27.5% in the southeast part of CEC from 2000 to 2005, which was higher than in other parts of the study region (He et al., 2007). Wang et al. (2006a) reported that the transported Beijing plumes superimposed on regional pollution sources was the dominant mechanism causing high ozone concentrations at a rural site in northern CEC in June–July 2005. Wang et al. (2006b) and Li et al. (2007) also found that regional-scale transport contributed not only to high ozone levels during certain events, but also to the monthly mean ozone concentrations. The inter-continental transport of ozone from CEC in summer also has been reported in some recent work (Pochanart et al., 2004; Zhu et al., 2004).

The goal of this study was to better understand the sources and transport of regional high ozone levels in CEC and to reduce the possibility of the occurrence of high ozone events in the future. To address these issues, systematic research at a representative site over CEC and quantitative evaluation of the contributions of regional-scale transport from various ozone production regions were conducted.

To study ozone chemistry/transport and aerosol composition/chemistry/transport over CEC, the Frontier Research Center for Global Change (FRCGC), the Japan Agency for Marine-Earth Science and Technology (JAMSTEC), the Institute of Atmospheric Physics (IAP), and the Chinese Academy of Sciences (CAS) conducted a field campaign – the Mount Tai eXperiment 2006 (MTX2006). The goal of MTX2006 was to conduct regional ozone photochemistry and aerosol studies in CEC at Mt. Tai ( $36.25^\circ$  N,  $117.10^\circ$  E,

1534 m a.s.l., an isolated single mountain in the middle of CEC) in June 2006, when the highest monthly mean ozone occurred. The concentration of surface  $O_3$ , CO,  $NO_x$ , VOCs, elemental carbon (EC), and organic carbon (OC); the chemical compositions of aerosols,  $J$  values, the tropospheric  $NO_2$  column, and meteorological variables were measured. Akimoto et al. (2008) and Kanaya et al. (2008) provide details about the procedures used to conduct this experiment, the sampling instruments, and the evolution of the composition of trace gases. The monthly mean ozone level measured in this study (85 ppbv) was the highest in recent years; it was 78 ppbv in 2004 (Li et al., 2007) and 55 ppbv in 2003 (unpublished data).

The main objective of this study was to identify the regions in which high ozone levels are produced over CEC. The focus was to quantitatively evaluate the contributions of regional-scale transport from various ozone production regions to the accumulation and distribution of ozone over CEC in a regional context. The transport of ozone from China to outflow regions of East Asia was examined using an Eulerian regional chemical model, the Nested Air Quality Prediction Modeling System (NAQPMS), with an on-line tracer tagging module. This study also provided a prototype of how to analyze model uncertainties. A brief description of the regional chemical transport model and the on-line tagged-tracer approach are presented first, followed by evaluation of the model through a comparison of simulations with observations from the MTX2006 field campaign. The contributions from various ozone production regions then are quantitatively evaluated. Finally, contributions of the near-ground ozone from CEC to East Asia are discussed.

This paper appears to be the first attempt to provide a quantitative analysis of the impacts of ozone from various ozone production regions within CEC. The results should provide valuable insights for policy makers to help decrease the ozone levels in this region.

## 2 Model description

To differentiate the contributions from various ozone production regions to total ozone levels over CEC, we applied a tagged tracer method developed by Wang et al. (2008) in the framework of NAQPMS. Compared with the classic sensitivity analysis that turns on and off emissions in targeted ozone production regions, the tagged tracer method provides a different and more efficient measurement of the relative importance of various ozone production regions and lacks the errors introduced by important non-linearities in the transport and fast photochemistry of ozone and its precursors. A similar approach was used by Wang et al. (1998) and Sudo and Akimoto (2007). Details about the model and the tagged tracer module are given in the following subsections.

## 2.1 Regional chemical transport model

Previous publications provided a detailed description of the NAQPMS used in this study (Li et al., 2007; Wang et al., 1996, 2000, 2001b, 2006b). Briefly, the NAQPMS is implemented in two steps: a mesoscale meteorological model to generate the wind field and a nested chemical transport module. The meteorological model is a 3-D non-hydrostatic mesoscale modeling system, which is called the fifth generation Mesoscale Model (MM5) and was developed by researchers at Penn State University and the National Center for Atmospheric Research (NCAR) (Grell et al., 1994). The initial and boundary conditions for MM5 are from NCAR/NCEP  $1^\circ \times 1^\circ$  reanalysis data at 6-h intervals. The nested chemical transport module includes advection/convection and diffusion processes, gas/aqueous chemistry, parameterization of dry/wet deposition, and a unique dust particle deflation module (Wang et al., 2000, 2002; Zhu et al., 2004). Carbon-Bond Mechanism Z (CBM-Z), which is composed of 133 reactions for 53 species, was applied in NAQPMS. Compared with Carbon-Bond IV, the CBM-Z extends the framework to function properly at larger spatial and longer time scales (Zaveri and Peters, 1999). The advection scheme employs a simplified but accurate mass-conserving, peak-preserving, mixing ratio-bounded advection algorithm (Walcek and Aleksic, 1998). The dry deposition module was updated to Wesely's scheme (1989). Since 1995, the NAQPMS has been used successfully to model dust events (Wang et al., 2000), the transport of and chemical processes within polluted air masses (Sulfur,  $O_3$ ) (Li et al., 2007; Wang et al., 2000, 2006b; Zhu et al., 2004), and the interactions between mineral aerosols and acid rain over East Asia (Wang et al., 2002).

Figure 1 shows the model domain of the NAQPMS simulation used in this study, which is composed of two nested domains. The coarser domain is  $6075 \text{ km} \times 4620 \text{ km}$  on a Lambert conformal map projection with 81-km grid resolution. The nested domain is divided into  $72 \times 69$  horizontal grids with 27-km resolution. Mt. Tai sits in the center of the inner domain. Vertically, the model uses ten terrain-following layers, five of which are within the lowest 1 km above the surface. Vertical grid spacing is increased gradually from 50 m at the surface to 2000 m at the top (10 km a.s.l.).

The anthropogenic emission inventory (fossil fuels, bio-fuels, and industrial emissions, excluding biomass burning) used in this study was derived from the 2006 bottom-up Regional Emission inventory in ASia (REAS) data with  $0.5^\circ \times 0.5^\circ$  resolution; these data were based on several energy statistics, emission factors, and economic information (Ohara et al., 2007). More detailed information about the emission inventory can be found in Yamaji et al. (2008). In this study, REAS emissions were mapped onto a  $0.1^\circ \times 0.1^\circ$  grid using the distribution of Streets' inventory (personal communication) with  $0.1^\circ$  resolution. The biomass burning emission inventory of China was based on the work

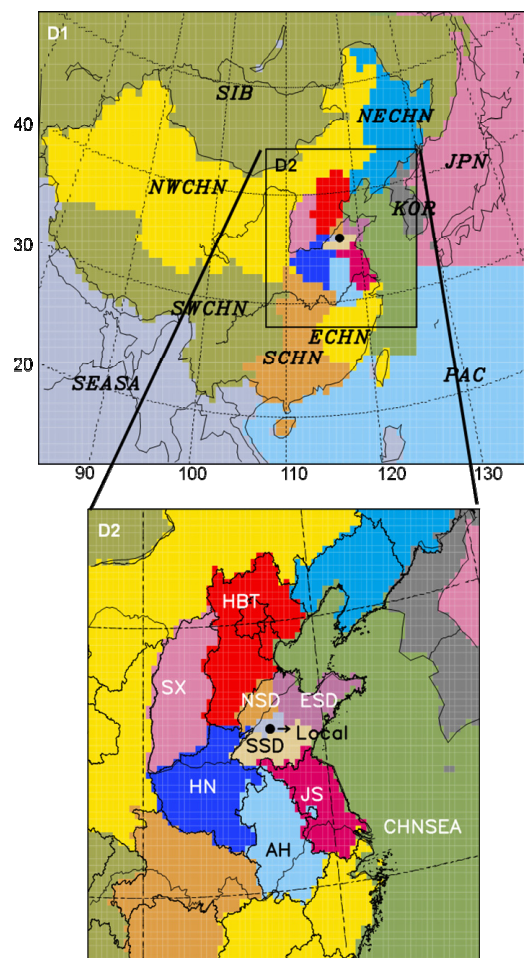


**Fig. 1.** Two nested model domain for NAQPMS used in this study. Also shown are regional separations for tracer tracer-tagged (characters). The marked solid circle represents the location of Mt. Tai. CEC consists of Local, SSD, ESD, NSD, HBT, SX, HN, AH, JS and CHNSEA.

of Cao et al. (2005), who provided a provincial resolution inventory that included sulfur dioxide ( $SO_2$ ),  $NO_x$ ,  $CH_4$ , CO, black carbon (BC), organic carbon (OC), and VOCs. Biomass burning emissions were projected onto a  $1^\circ \times 1^\circ$  grid and based on the Global Fire Emissions Database version 2 (GFEDv2) (van der Werf et al., 2006) that was resampled to an 8-day time step using MODIS fire hot spots (Giglio et al., 2003) with  $1^\circ \times 1^\circ$  resolution by calculating the relative fractions of emissions on every grid in one province in GFEDv2. Data about the emissions of countries other than China came directly from GFEDv2. Biogenic hydrocarbon emissions data came from the Global Emissions Inventory Activity (GEIA) (Guenther et al., 1995).

The simulation started at 08:00 UTC on 1 May 2006 and ran through the end of June 2006. The first 14 days are regarded as the spin-up period to reduce the influence of initial conditions. The initial, lateral and top boundary conditions

**Table 1.** Tagged ozone production regions in East Asia.

Regions <sup>a</sup>	Description
Local	Tai'an and Lai'wu city, ShanDong province, China
SSD	Southern ShanDong province, China
ESD	Eastern ShanDong province, China
NSD	Northern ShanDong province, China
HBT	Hebei, Beijing, and Tianjin, China
SX	ShanXi province, China
HN	HeNan province, China
AH	AnHui province, China
JS	JiangSu province, China
CHNSEA	CHiNa SEA, including Bohai Sea, Huanghai Sea and East Sea
NECHN	NorthEast CHiNa, including Heilongjiang, Jilin and Liaoning provinces, China
ECHN	East CHiNa, including Shanghai, Zhejiang, Fujian, Jiangxi and Taiwan provinces, China
SCHN	South CHiNa, including Hubei, Hunan, Guangdong, Guangxi, Hainan and Hong Kong provinces, China
SWCHN	SouthWest CHiNa, including Sichuan, Chongqing, Guizhou, Yunnan, and Tibet provinces, China
NWCHN	NorthWest CHiNa, including Shanxi, Gansu, Qinghai, Ningxia, Xinjiang, and Neimenggu provinces, China
KOR	KORea
JPN	JaPaN
SIB	SIBeria
PAC	western PACific rim
SEASA	SouthEast ASiA

<sup>a</sup> Locations of regions are shown in Fig. 1.

of several chemical species ( $O_3$ ,  $CO$ ,  $NO_x$ , ethane, and propane) were provided by the 3-hourly outputs from a coupled tropospheric chemistry climate model CHASER (Sudo et al., 2002) with  $2.8^\circ \times 2.8^\circ$  horizontal resolution.

## 2.2 Tracer tagging

$O_3$  was labeled by the geographical location in which it was formed.  $O_3$  from the top and lateral boundaries and from initial conditions also were tagged. The fraction of any tagged ozone ( $O_3^T$ ) in total ozone was calculated at a 5-min time step. We assumed that different phases of  $O_3^T$  were mixed well within each grid cell and that each  $O_3^T$  shared the same loss coefficients as total ozone (including outflow, chemical destruction, and dry and wet depositions), so that the fraction of each tagged ozone at any given grid cell cannot be changed by removal processes, and is calculated as follows:

$$\left( \frac{dFO_3^T}{dt} \right)_{ij} = \left( P_{ij} + (M_{ij})_{\text{dif+adv+conv}} \right) / O_3 \quad (1)$$

where  $i$  and  $j$  represent the  $i$ th geographical source region and the  $j$ th grid cell, respectively;  $FO_3^T$  is the fraction of the  $i$ th  $O_3^T$  in  $j$ th grid cell; and  $P_{ij}$  is the gross photochemical ozone production of the  $i$ th source region in the  $j$ th grid cell. Here, if the  $j$ th grid cell is within the tagged geographical source region  $i$ ,  $P_{ij}$  is calculated as described in Davis et al. (2003) and Kondo et al. (2004). Otherwise,  $P_{ij}$  is equal to zero (outside region  $i$ ).  $(M_{ij})_{\text{dif+adv+conv}}$  is the  $O_3^T$  inflow

from the adjacent grid cells due to advection, diffusion, and convection and is calculated by the inflow fluxes and the  $i$ th  $O_3^T$  fraction in those adjacent grid cells.  $O_3$  is the mixing ratio of total ozone. It can be easily shown that the contributions of labeled ozone to the total are strictly positive, which is different from the classic sensitivity approach.

In this study, 20 ozone production regions in East Asia were tagged, as were lateral and top boundaries ozone and initial ozone. Figure 1 and Table 1 show the location and description of each region in CEC. Local refers to Tai'an and Laiwu City, a region with a  $1 \times 10^5 \text{ km}^2$  area, 6.6 million people, and Mt. Tai. SSD, ESD, and NSD are the southern, eastern, and northern parts of ShanDong Province, respectively. HBT includes Hebei Province, Beijing, and Tianjin City, where the steel industry and traffic are the major emitters of ozone precursors in China. SX represents ShanXi Province, which is the biggest coal producer in China (248.9 million tons per year, 25% of the country's total). HN (HeNan Province) boasts the largest population in China (97.7 million). AH and JS represent AnHui and JiangSu Provinces, which have the most developed petrochemistry industries in China. Finally, CHNSEA includes the Bohai Sea, the Huanghai Sea, and the East China Sea, which are all close enough to CEC to influence the outflow of CEC ozone precursors, which could further affect the ozone mixing ratios.

Table 2 lists the monthly  $NO_x$  emissions of the 10 regions within CEC. Biomass burning emissions with an 8-day time step also are shown to illustrate their high temporal

**Table 2.** Model NO<sub>x</sub> emissions in Ton NO<sub>2</sub>/month from the major regions over CEC.

Regions <sup>a</sup>	Anthropogenic <sup>b</sup>	BB <sup>c</sup>	BB1 <sup>c</sup>	BB2 <sup>c</sup>	BB3 <sup>c</sup>	BB4 <sup>c</sup>	Area <sup>d</sup>
Local	8659	3623	876	1665	1025	57	1.0
SSD	20 633	55 525	13 508	37 697	3006	1314	5.1
ESD	18 833	21 845	5052	10 230	3970	2593	6.9
NSD	16 772	6837	1214	1661	3929	33	2.7
HBT	126 810	16 269	261	5089	9127	1892	21.8
SX	59 131	5586	1143	1830	1809	804	15.6
HN	69 522	52 279	33 243	15042	3841	153	16.7
AH	51 021	54 465	20 728	33 065	530	142	13.9
JS	97 156	77 279	12 268	62 355	2567	89	10.3
CHNSEA	0	0	0	0	0	0	0
Total	468 537	293 708	85 493	164 634	25 804	5319	94

<sup>a</sup> Region names are shown in Fig. 1.

<sup>b</sup> Anthropogenic emissions include fossil fuel, biofuel, industrial excluding open biomass burning.

<sup>c</sup> BB is the monthly emissions from Biomass burning in Ton NO<sub>2</sub>/mon. BB1, BB2, BB3, and BB4 represent the emissions during 2–9, 10–17, 18–25, and 26–30 June from biomass burning. Units are Ton NO<sub>2</sub>/8days.

<sup>d</sup> Unit is 10<sup>5</sup> square kilometers.

variability. Biomass burning contributed NO<sub>x</sub> emissions comparable to those from anthropogenic activities in the southern parts of CEC, especially during the first 16 days of June, which exerted an influence on the ozone concentrations in CEC.

### 3 Model evaluation

#### 3.1 Observed ozone and related species at Mt. Tai

Figure 2 presents the time series of hourly averaged concentrations of O<sub>3</sub>, CO, NO<sub>x</sub>, and BC at Mt. Tai. The air quality at Mt. Tai during the study period was not good. Over the 30 days, 14 days had hourly ozone mixing ratios that exceeded 100 ppbv China's air quality standard (Grade II). The observed mean O<sub>3</sub> concentration (82 ppbv) not only was 30 ppbv higher than observations at the rural/remote sites over the North Pacific (Pochanart et al., 2004), but also higher than the previous modeled results for this particular location (Yamaji et al., 2006; [http://www.atmos.washington.edu/~jaegle/geoso3\\_start.html](http://www.atmos.washington.edu/~jaegle/geoso3_start.html)). The mean concentrations of CO and BC reached 560 ppbv and 3.4 μg C/m<sup>3</sup>, both of which were higher than the satellite observations ([http://mopitt.eos.ucar.edu/mopitt/data/plots/mapsv3\\_mon.html](http://mopitt.eos.ucar.edu/mopitt/data/plots/mapsv3_mon.html)).

In this study, two high pollution episodes are defined: 16:00 UTC on 5 June to 16:00 UTC on 7 June (Case I) and 04:00 UTC on 11 June to 11:00 UTC on 13 June (Case II). The mean concentrations of O<sub>3</sub>, CO, NO<sub>x</sub>, and BC in Case II reached 95 ppbv, 700 ppbv, 2.5 ppbv, and 8 μg C/m<sup>3</sup>, with maximums of 160 ppbv, 1700 ppbv, 8 ppbv, and 20 μg C/m<sup>3</sup>, respectively. In the following sections, we examine the ozone production regions and transport of ozone, focusing on these two cases. Furthermore, to better understand the

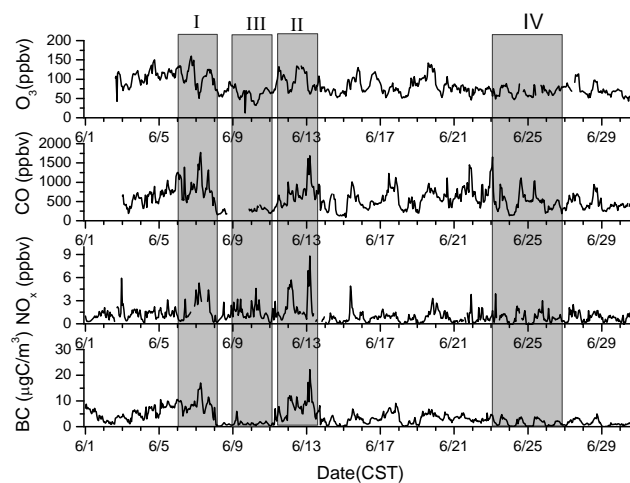


**Fig. 2.** Observed hourly averaged O<sub>3</sub>, CO, NO<sub>x</sub> and BC at Mt. Tai in June 2006. Four cases are marked by the semi-transparent shaded.

sources of the high level pollutants, we selected another case (16:00 UTC on 8 June to 23:00 UTC on 10 June; Case III) as a representative clear case, when the concentration of O<sub>3</sub>, CO, NO<sub>x</sub>, and BC were 64 ppbv, 276 ppbv, 1.3 ppbv, and 1.3 μg C/m<sup>3</sup>, respectively. The period from 00:00 UTC on 23:00 to 23:00 UTC on 26 June is considered as Case IV because of its typical meteorological pattern (Mei-Yu front), which frequently appears in CEC in summer.

#### 3.2 Comparison of model results and observations

Figure 3a shows the time variations of the predicted and observed hourly averaged meteorological and chemical

**Table 3.** Statistical summary of comparisons of the model results with observations

	N <sup>b</sup>	C <sub>mod</sub> <sup>c</sup>	C <sub>obs</sub> <sup>c</sup>	NB	RMSE	R
<i>Mt. Tai</i>						
O <sub>3</sub>	666 (28)	85	82	3.7 (4.0)	22.3 (14.2)	0.56 (0.69)
CO	641 (28)	417	560	-125.1 (-120.5)	378.6 (265.8)	0.25(0.46)
NO <sub>x</sub>	681 (28)	1.2	1.1	0.1 (0.1)	1.2 (0.6)	0.30 (0.62)
BC	720 (28)	2.7	3.4	-0.6 (0.6)	3.4 (2.3)	0.41 (0.62)
<i>Yonaguni</i>						
O <sub>3</sub>	719 (30)	24	24	1.1 (0.7)	11.2 (9.0)	0.82 (0.93)
CO	703 (30)	75	112	-38.1 (-43.9)	57.9 (55)	0.81 (0.87)

<sup>a</sup> Values in bracket denote daily mean concentrations. Others are hourly mean concentrations.

Units are ppbv except for BC which is  $\mu\text{g C/m}^3$ .

<sup>b</sup> N is the number of observed samples. For model results, N is 720 h and 30 days.

<sup>c</sup> C<sub>mod</sub> and C<sub>obs</sub> represent the modeled (all hours) and observed mean concentrations (lacked hours are omitted).

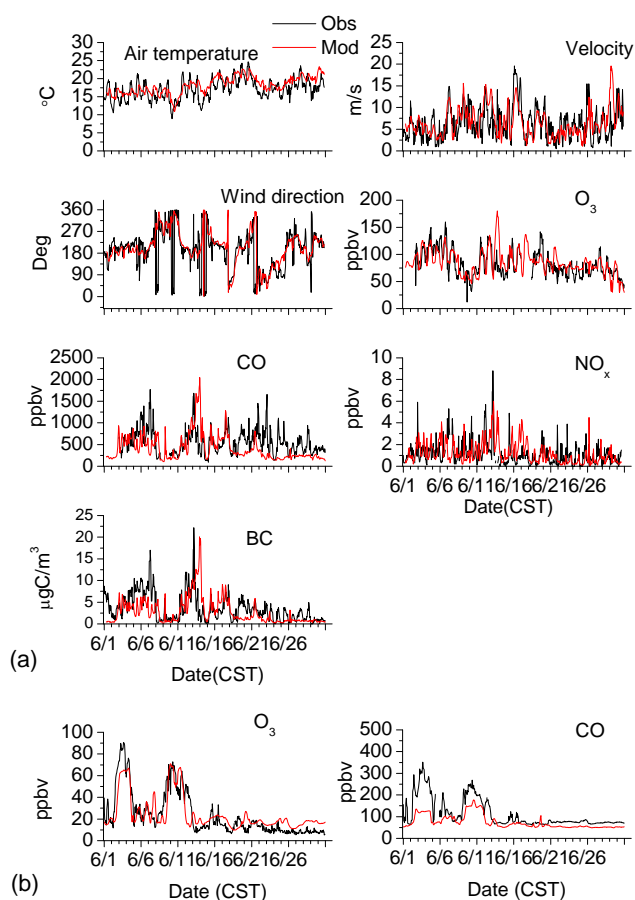


**Fig. 3.** Time profile of the model predicted and observed meteorological and chemical parameters during June 2006 at (a) Mt. Tai, (b) Yonaguni (123.02° E, 24.47° N, 30 m a.s.l.).

variables at Mt. Tai. The model reproduced the synoptic features of the meteorological variables, notably the change of wind direction from northward to southward during the two

heavy pollution episodes. The simulated time series of ozone concentration was generally satisfactory, as the model effectively reproduced the daily variations. The correlation coefficients of hourly and daily ozone concentrations between the modeled and observed values were 0.56 and 0.69, respectively (Table 3). The simulated monthly mean ozone (85 ppbv) showed that the model captured the same magnitude as the observations, which is confirmed by the small mean bias (MB) and the root mean square error (RMSE) of the hourly and daily mean ozone concentrations (Table 3). NO<sub>x</sub> concentrations also were well reproduced by the model. The simulated correlation, NB, and RMSE of daily mean NO<sub>x</sub> were 0.62, 0.1 ppbv, and 0.50 ppbv, respectively. General agreement also occurred between the observed and simulated BC and CO trends, with correlations of 0.62 and 0.46, respectively. Note that CO and BC were systematically underestimated in the latter part of MTX2006; this pattern also has been seen in other modeling studies for the coastal area of China, where the transport of high CO concentration (>500 ppbv) from CEC was underestimated (Zhang et al., 2003). The underestimation likely is due to the uncertainties of the emission databases. Streets et al. (2003) reported 156% and 484% uncertainties in China's CO and BC emissions, and Wang et al. (2004) indicated that the emissions of CO in 2000 were substantially (>80%) underestimated over CEC in a bottom-up inventory performed by comparing model results with observations at stations in CEC and flights in the Asia Pacific rim. Recent work by Streets (D. G. Streets, personal communication) showed a 300% increase of CO emissions in the industry sector in CEC since 2000.

The model simulations reproduced both high pollution cases (Fig. 3a). In Case I, the simulation underestimated the mixing ratios of pollutants but captured the trend well. The modeled O<sub>3</sub>, CO, NO<sub>x</sub>, and BC were 100 ppbv, 523 ppbv, 1.7 ppbv, and 3.9  $\mu\text{g C/m}^3$ , respectively, which were less than the observed values of 110 ppbv, 902 ppbv, 1.9 ppbv, and 8.7  $\mu\text{g C/m}^3$ . This difference was caused by the coarse time

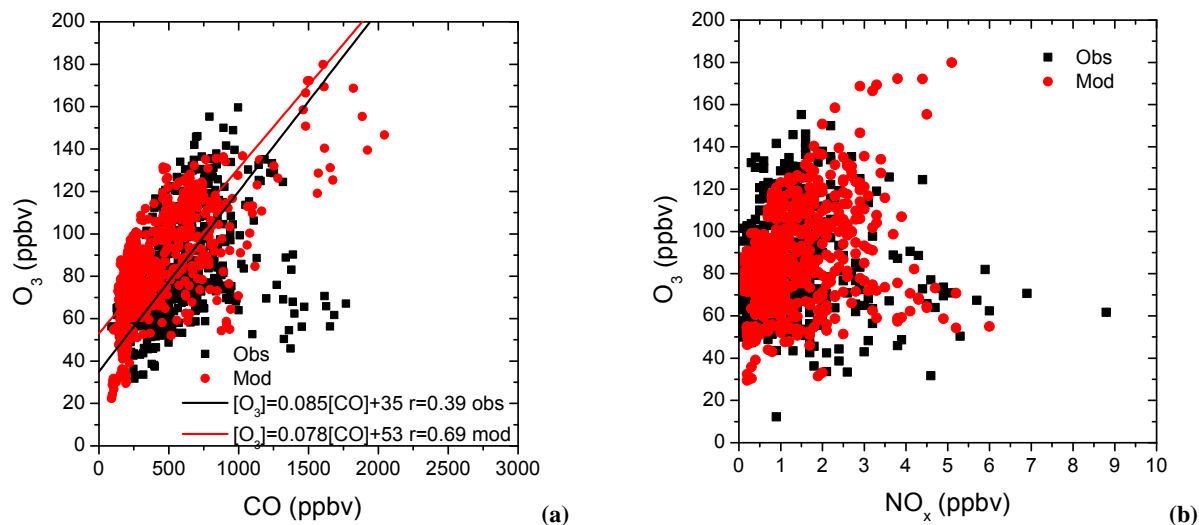


**Fig. 4.** Scatter plots of  $O_3$  vs. (a) CO and (b)  $NO_x$  observed (solid squares) and predicted by the model (solid circles) at Mt. Tai in June 2006. The regression statistics are determined by the reduced major axis method.

and grid resolutions of the biomass burning emissions. As shown in Table 2, intensive burning activities occur to the south of Mt. Tai, especially in the SSD region, which is only 150 km away from the observation site. The coarse resolution of  $1^\circ$  and 8 days of the inventory made it hard to precisely represent the inhomogeneous spatial and temporal distributions of real emissions. In Case II, the simulated  $O_3$ , CO,  $NO_x$ , and BC were 97 ppbv, 729 ppbv, 2.6 ppbv, and  $6.7 \mu\text{g C/m}^3$ , respectively, which are close to the observed values of 98 ppbv, 734 ppbv, 2.5 ppbv, and  $8.2 \mu\text{g C/m}^3$ . The model also produced non-observed peaks of ozone at 10:00 UTC on 13 June, likely because of a discrepancy with the modeled winds. After 13 June, the observed wind changed its direction from south to west or north and brought in clear air masses. However, the modeled wind remained northward until 14 June and transported large amounts of ozone from south of Mt. Tai, where a large quantity of pollutants were emitted from biomass burning (Table 2).

Figure 4 shows the observed and modeled correlations between  $O_3$  and its precursors (CO and  $NO_x$ ) at Mt. Tai; these data help to assess the model performance in terms of photochemical processes. We applied the reduced major axis (RMA) regression method to calculate the slope, intercept, and correlation coefficient, rather than the standard linear least squares regression analyses because both ozone and its precursors are subjected to errors of measurement. Clearly, the simulated regression line between  $O_3$  and CO agrees with the observed one. Compared with its outflow region (the North Pacific, 0.12–0.35 ppbv/ppbv), Mt. Tai shows a smaller slope of  $O_3$  versus CO (model: 0.078 ppbv/ppbv; observation: 0.085 ppbv/ppbv) (Pochanart et al., 1999; Tanimoto et al., 2002) because of shorter transport time. The correlation between  $O_3$  and  $NO_x$  is quite different.  $O_3$  and

$NO_x$  generally were positively correlated during a low  $NO_x$  (<2.0 ppbv) period, whereas the relationship became negative under a high  $NO_x$  (>4.0 ppbv) condition. This pattern was well reproduced by the model.

The model simulations were validated further by comparing the model results with concentrations of  $O_3$  and CO observed at Yonaguni ( $123.02^\circ \text{ E}$ ,  $24.47^\circ \text{ N}$ , 30 m a.s.l.) (Fig. 3b). Yonaguni is a sea-level station located in the western Pacific Ocean in the network of the World Data Centre for Greenhouse Gases (WDCGG) (<http://gaw.kishou.go.jp/wdcgg/>). As shown in Fig. 3b and Table 3, temporal variation of the hourly mean concentrations was reproduced satisfactorily, although CO was underestimated.

The model also reproduced well the spatial and temporal variations of the observed ozone concentrations and ozone's precursors during the study period. This result provides confidence in the model-derived contributions of CEC ozone from different ozone production regions in this study.

## 4 Attribution of origins of near-ground ozone over CEC

### 4.1 Monthly mean attributions

Figure 5 illustrates the modeled monthly mean  $O_3$  concentrations (shaded) and wind fields (arrows) in the lower troposphere (below 1.5 km) in June 2006. During this time period, CEC was covered with air masses with high ozone concentrations (65–85 ppbv). Mt. Tai was in the center of a high ozone region with prevailing northward wind. In this section, we analyze the results of the simulated tagged  $O_3$  to examine the source region of ozone, focusing on the contributions of each area and the role of regional transport.

**Table 4.** Contributions to ozone mixing ratios at Mt. Tai from selected ozone production regions.<sup>a</sup>

Regions	Monthly mean	Case I	Case II	Case III	Case IV
Local	9.8 (11.5)	9.3 (9.3)	7.0 (7.2)	12.1 (18.3)	5.7 (8.4)
ESD	1 (1.2)	0.1 (0.1)	0 (0)	0 (0)	1.0 (1.5)
SSD	18.5 (21.5)	29.8 (29.8)	27.6 (28.5)	2.9 (4.2)	7.0 (10.4)
NSD	2.2 (2.6)	0.1 (0.1)	0 (0.1)	8.5 (12.9)	0.5 (0.7)
HBT	1.5 (1.8)	0.2 (0.2)	0.5 (0.5)	7.5 (11.3)	0.6 (0.9)
SX	0.4 (0.5)	0.1 (0.1)	0.6 (0.6)	1.2 (1.8)	0.3 (0.5)
HN	2.8 (3.3)	1.0 (1.0)	3.6 (3.7)	1.1 (1.6)	2.2 (3.3)
AH	5.6 (6.6)	6.6 (6.6)	12.8 (13.2)	0.7 (1.1)	2.1 (3.1)
JS	8.3 (9.8)	14.8 (14.8)	18.8 (19.4)	1.0 (1.6)	1.2 (1.8)
CHNSEA	1.3 (1.5)	1.0 (1.0)	0.7 (0.7)	0.1 (0.2)	2.2 (3.3)
Inner <sup>b</sup>	51.4 (60.2)	63.1 (63.1)	71.7 (73.8)	35.2 (53.0)	22.8 (33.9)
Outer <sup>b</sup>	3.1 (3.7)	3.0 (3.0)	2.4 (2.5)	1.6 (2.5)	3.6 (5.3)
Boundary <sup>c</sup>	14.0 (16.4)	12.2 (12.1)	11.9 (12.2)	19.9 (30.0)	16.2 (24.1)
Upper <sup>c</sup>	16.7 (19.6)	21.8 (21.8)	11.1 (11.4)	9.6 (14.5)	24.7 (36.7)
Total	85.4 (100)	100.1 (100)	97.2 (100)	66.3 (100)	67.3 (100)

<sup>a</sup> Units are ppbv with percentages indicated in brackets.

<sup>b</sup> Inner is the sum of 10 ozone production regions in CEC, and outer is the sum of the other regions.

<sup>c</sup> Boundary and Upper represent the contributions from lateral and top boundary conditions.

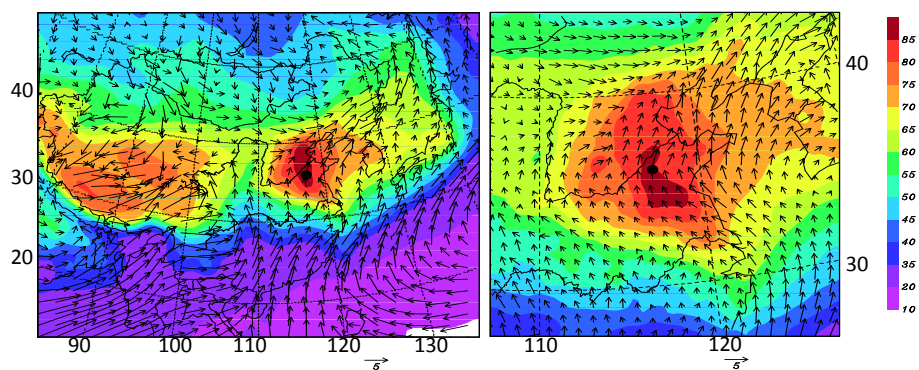


**Fig. 5.** Simulated monthly mean near-ground (<1.5 km) ozone (ppbv, shaded) and wind vector (m/s, arrows) in June 2006 in two domains (Left: Domain1; Right: Domain2). Mt. Tai is marked by the dark solid circles.

Table 4 shows the estimated contributions to ozone mixing ratios of the selected ozone production regions at Mt. Tai (Fig. 1, Table 1). To better describe the interactions between different regions in CEC, we provide the results for each region in CEC and treat the other ozone production regions as the outer region (Outer, which includes SIB, NWCHN, SWCHN, SCHN, ECHN, NECHN, PAC, KOR, JPN, and SEASA).

In general, the photochemical production of ozone within CEC was the most important mechanism, leading to a monthly mean ozone mixing ratio of 51.4 ppbv (60.2%). The ozone results from photochemical production over the other regions and from the lateral and top boundary were 3.1 (3.7%), 14.0 (16.4%), and 16.7 ppbv (19.6%), respectively. Table 4 indicates that regional transport played the major role (41.6 ppbv and 48.7%) in creating the high O<sub>3</sub> concentrations

at Mt. Tai, as opposed to local photochemical production (9.8 ppbv and 11.5%), which agrees well with the results of Kanaya et al. (2008). They found that in situ photochemical production did not exhibit large differences between high and low ozone cases at the station. Ozone formed in SSD, AH, and JS contributed the greatest fraction (32.4 ppbv and 37.9% of total ozone) to the total, likely because of high emission rates and favorable meteorological conditions in those areas. These areas also exhibited high NO<sub>x</sub> anthropogenic emissions (Table 2) and, due to heavy post-harvest agricultural waste burning activities (Fu et al., 2007), a large amount of pollutants (even more than anthropogenic emissions) were emitted (Table 2). Under northwestward wind conditions (Fig. 5), the large quantities of ozone formed in these regions were transported to Mt. Tai.

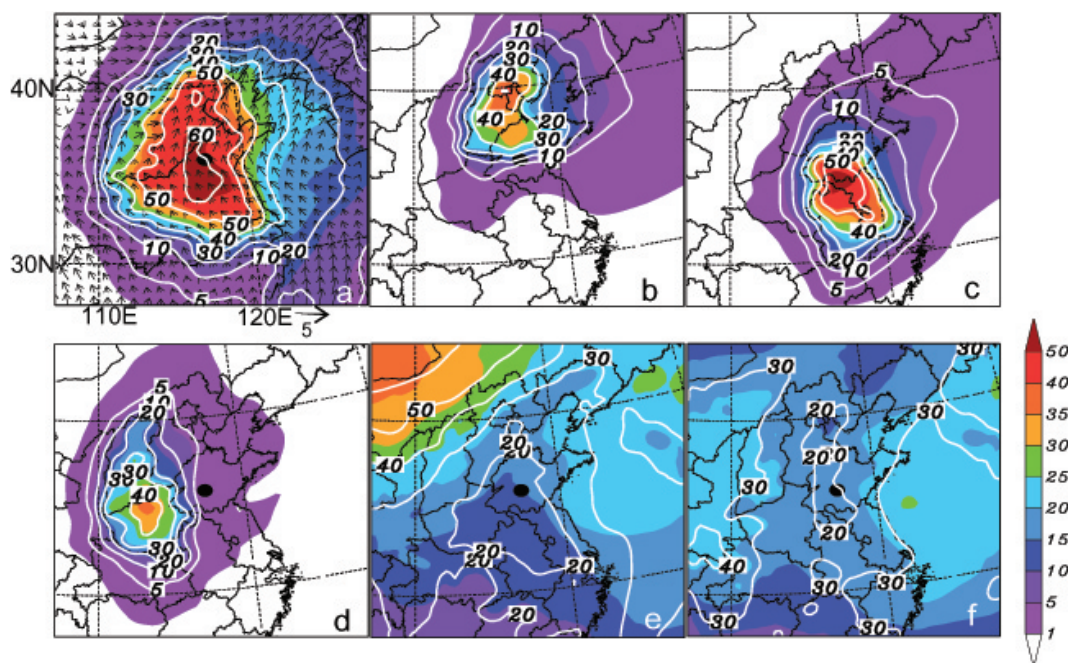


**Fig. 6.** Spatial distributions of contributions (shaded: ppbv; contours: %) to monthly mean near-ground (<1.5 km) ozone in June in CEC from (a) all photochemical production inner CEC, (b) HBT+NSD+ESD+Local, (c) SSD+AH+JS, (d) SX+HN, (e) Lateral boundary, and (f) top boundary. Mt. Tai is marked by the dark solid circles.

Figure 6 shows the horizontal distribution of monthly mean contributions to near-ground ozone from photochemical reactions in different sources regions and from the lateral and top boundaries. In this study, photochemical production in CEC accounted for 25–60 ppbv (30–70%) of  $O_3$  in the geographical distribution. The highest concentration of chemically produced  $O_3$  (55 ppbv, 60%) occurred to the south of Mt. Tai (Fig. 6a). The contributions from lateral and top boundaries were 10–20 and 15–25 ppbv over CEC, respectively (Fig. 6e, f), with minimal contributions in polluting regions and maximal contributions in remote areas. Due to the effect of regional transport, the influenced areas around an  $O_3$  forming source region expanded remarkably. For example, chemically produced ozone from the south of CEC (SSD + AH + JS) was transported northeastwardly to HBT, where the contribution of transport reached ~5–10 ppbv (5–15%) (Fig. 6c). Similarly, ozone chemically produced in the Local, NSD, ESD, and HBT areas was transported out of CEC to the northeast of China (Fig. 6b).

Our data show a little higher contribution of photochemical reactions to total ozone levels over CEC (25–60 ppbv, 30–70%) than the estimates (15–30 ppbv and 30–60%) made by Yamaji et al. (2006), who made their estimate by turning off all emissions. Similar higher estimates were found in the study of Derwent (2004) by a tracer-tagged technique. The on-line tracer-tagged technique used in this study estimated the contributions from different sources at the current ozone production rates resulting from sources combined. In our tracer-tagged technique, all contributions are strictly

positive. However, taking out a targeted region's emissions provides a more policy-relevant quantification by describing responses to emission controls that will change ozone production rates due to non-linearities of photochemistry. In a sensitivity approach, a negative impact often appears, particularly in highly emission regions in winter. For the contribution from the top boundary, the simulated result was similar to that reported by Wang et al. (1998). In their study, the zonal averaged contribution to near-ground ozone from the upper air (>400 hpa) in July between 30° N and 40° N was 15–25%.

#### 4.2 Attributions during the typical cases

Table 4 shows the estimated attributions during two high pollution cases (Case I and II) and a clean case (Case III) at Mt. Tai. Figure 7 presents the spatial distributions of contributions from different sources for the same time periods. Note that we selected these cases because of their representativeness for typical regional transport. As shown in Fig. 3, strong northward (Case I and II) and southward (Case III) winds at Mt. Tai suggest that these three time periods cover regional transport of both the southern and northern parts of CEC. The weather patterns that occurred during these cases have been reported to appear frequently in CEC in May–June (Wang et al., 2006).  $O_3$ , CO,  $NO_x$  and BC increased rapidly in cases I and II, and all contributed greatly to the maximum ozone concentration in June.

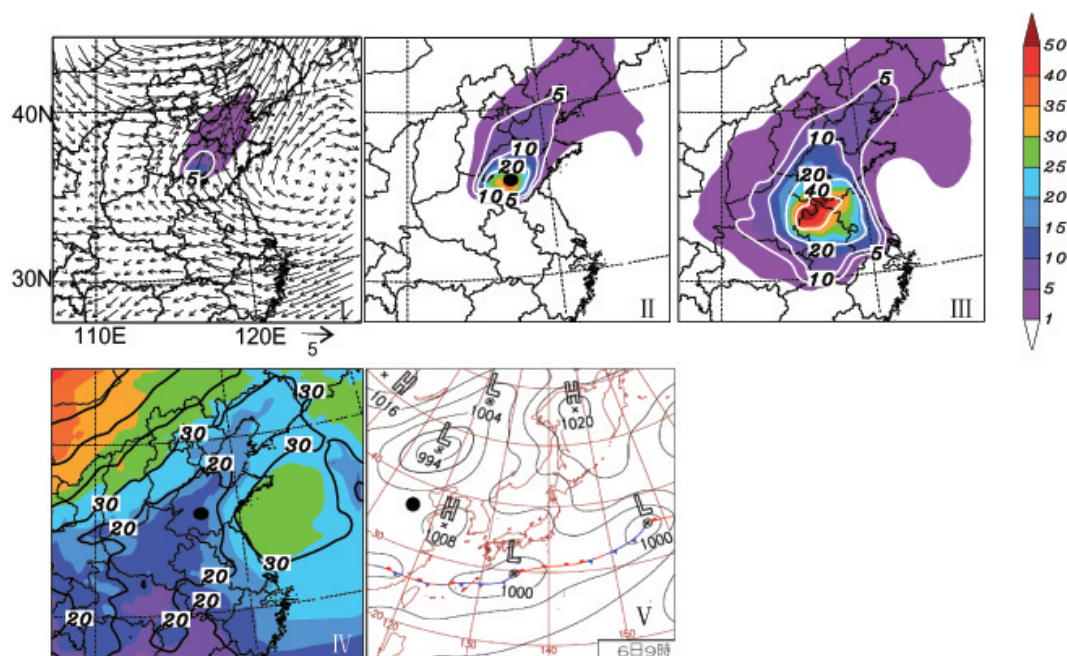


**Fig. 7a.** Spatial distributions of contributions (shaded: ppbv; contours: %) to near-ground (<1.5 km) ozone in Case I from I) Local, II) SSD, III) AH + JS and IV) Lateral Boundary. The surface weather chart (V) at 00Z06June (UTC), 2006 is also shown from Japan Meteorological Agency (<http://www.data.jma.go.jp/fcd/yoho/hibiten/index.html>).

Case I: The meteorological conditions over CEC were controlled by a stable high pressure system (1008 hpa) located over the East China Sea, which favored  $O_3$  photochemical production and northward transport (Fig. 7a). Intensive biomass burning activities occurred in the south of CEC (Table 2). In SSD and AH,  $NO_x$  emission rates from biomass burning were even higher than those from anthropogenic  $NO_x$ . As a result, the high levels of ozone that formed over SSD, AH, and JS were transported northward by the southern wind. At Mt. Tai, this transport contribution reached 52 ppbv, which was >50% of the total surface ozone levels (Table 4). High ozone events under similar meteorological conditions have been reported in previous work (Wang et al., 2006).

Case II: Mt. Tai lies between an inverse trough, located in Mongolia and Northwest China, and subtropical high pressure (Fig. 7b). Consequently, a strong southern wind prevails over CEC. Similar to Case I, strong biomass burning emissions covered SSD, JS, and AH (Table 2). Ozone levels formed in SSD and JS + AH were 5–40 ppbv (5–40%) and 10–70 ppbv (10–70%) over CEC, respectively, with 28 ppbv (29%) and 32 ppbv (33%) at Mt. Tai. Even in the Bohai Sea, the sum of transported ozone from SSD, AH, and JS reached ~20 ppbv (Fig. 7b). Table 4 shows that ozone produced within CEC reached 72 ppbv (74% of the total surface ozone concentrations) at Mt. Tai, in which the transport from SSD + AH + JS covered 59 ppbv (62% of total ozone).

Case III: Case III occurred on 8–10 June, a period between Cases I and II. The observed mean ozone level was only 64 ppbv, which was much less than those of Cases I and II. Figure 7c shows that CEC experienced strong low pressure (988 hpa), which moved in from Mongolia (Fig. 7a). This pattern resulted in the clean air mass from the north mixing with polluted air from HBT before arriving at Mt. Tai (Fig. 7c). Under the strong northwestern wind, ozone from the lateral boundary covered a large fraction of the northern CEC (Fig. 7c). The  $O_3$  chemically produced over HBT and NSD also was transported southward to Mt. Tai and reached 7.5 ppbv (11%) and 8.5 ppbv (13%), respectively. Compared with the data from Cases I and II, it is clear that less chemically produced ozone (35 ppbv), mainly from northern parts of CEC (HBT, NSD, and Local), was the major cause of low total ozone. It can be concluded that the transport of  $O_3$  generated by strong photochemical production from anthropogenic sources and biomass burning emissions in the southern parts of CEC (SSD, AH, and JS) played a key role in high ozone events at Mt. Tai.

These cases illustrate that the regional transport from southern CEC has great impacts on high ozone levels at Mt. Tai. To better investigate the role of transport, we compared them with Case IV during which the weather pattern suppressed regional transport of photochemically produced ozone. For this case (Table 4), the observed ozone was 67 ppbv, which is a much lower value than those of Cases I and II. The weather chart shows that a quasi-stationary

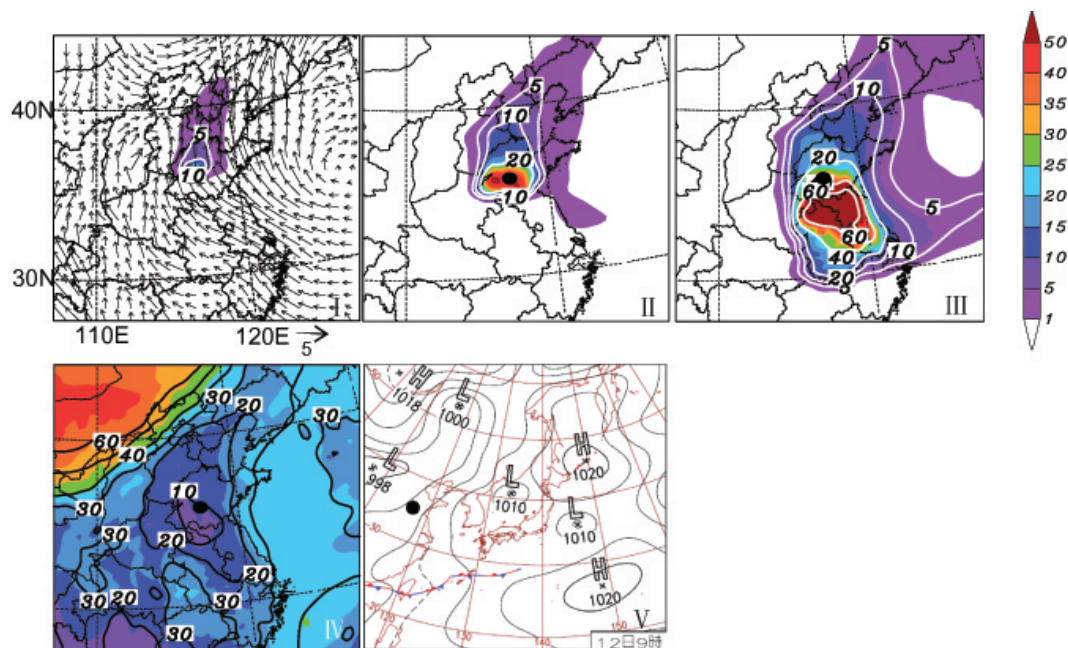


**Fig. 7b.** Same as Fig. 7a, but in Case II. And the surface weather chart is 00Z12June (UTC) 2006.

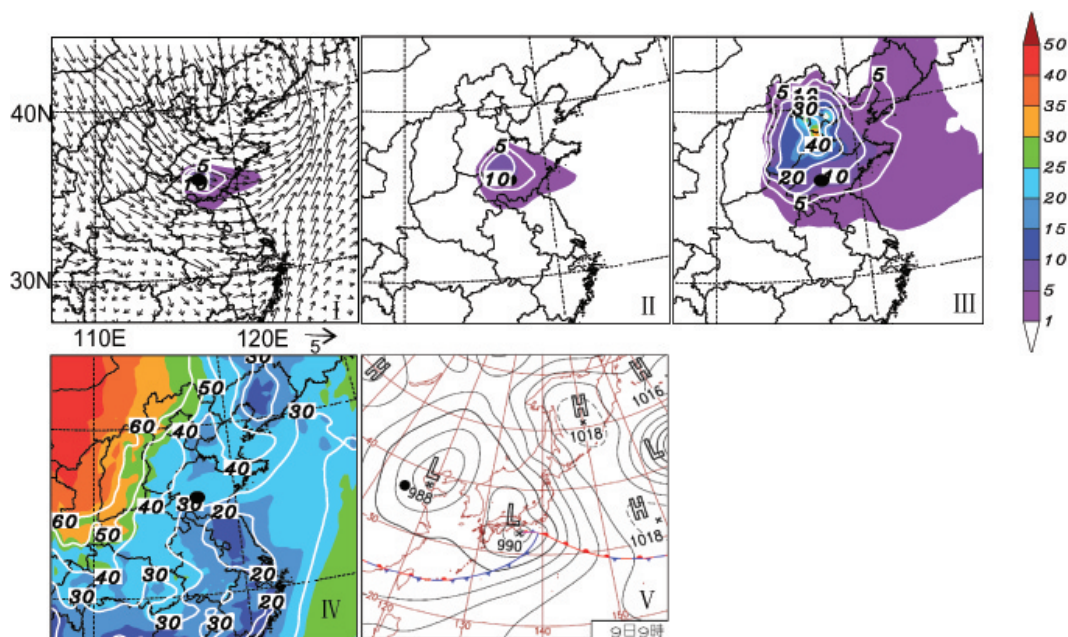


**Fig. 7c.** Same as Fig. 7a, but in Case III. The sources are: I) Local, II) NSD, III) HBT and IV) Lateral Boundary. And the surface weather chart is 00Z09June (UTC) 2006.

Mei-Yu front, a typical meteorological pattern in summer, stayed in the south of CEC (Fig. 7d). During this weather pattern, the low wind velocity at Mt. Tai (Fig. 3) suggests that less transport of ozone from other regions occurred. The simulated results indicated that the transport from southern CEC (SSD, AH, and JS) contributed only 15 ppbv (22%) to the total ozone at Mt. Tai, which was less than that in Cases I

(51 ppbv, 51%) and II (59 ppbv, 61%). This clearly suggests the important role of transport from southern CEC to create the June maximum at Mt. Tai. Compared with Cases I and II, the upper boundary during this period showed a higher contribution (24 ppbv), which likely was caused by severe mesoscale convection activity during the Mei-Yu season.

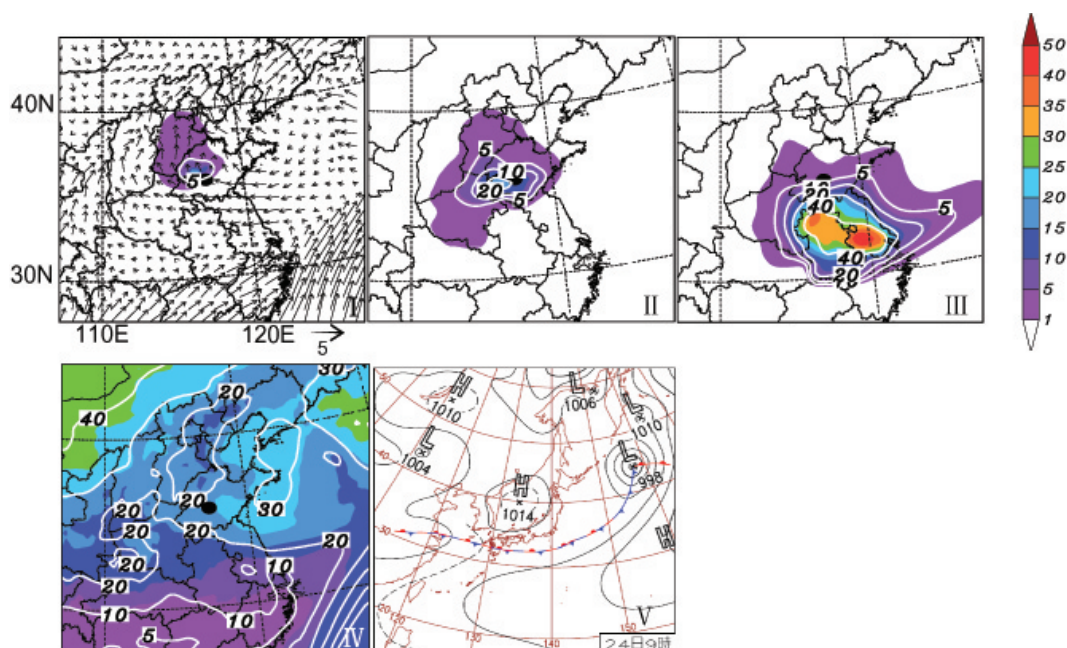


**Fig. 7d.** Same as Fig. 7a, but in Case IV. And the surface weather chart is 00Z24June (UTC) 2006.

We have demonstrated that  $O_3$  concentrations over CEC are controlled by photochemical production and that the regional transport from different ozone production regions within CEC, especially the southern parts (SSD, AH, and JS), plays an important role in the monthly mean  $O_3$  distributions and high ozone events. This transport from the southern parts of the CEC can even become the dominant mechanism that causes high ozone events in June at Mt. Tai.

#### 4.3 Error analysis

To estimate the uncertainties associated with the tracer-tagged technique, an error analysis is needed. Since the exact ozone contributions from the photochemistry in any targeted region are unknown, we conducted a second estimate in this study, as suggested by Grewe (2004): a comparison with the emission sensitivity approach which has been applied widely in studies of source apportionment. The error estimate ( $E_a$ ) for the  $i$ th geographical source region can be derived as follows:

$$E_a = C_i^t - C_i^s \quad (2)$$

where  $C_i^s$  and  $C_i^t$  represent the contribution (ppbv) of the  $i$ th geographical source region derived from the sensitivity approach and tracer-tagged technique, respectively. Note that the quality of the estimate of  $C_i^s$  can be tested by comparing the sum of the contributions of chemically produced ozone from all emissions in the whole model domain in the sensitivity analysis with the original ozone without any contributions from transport from the upper and lateral boundary ( $\sum C_i^t$ ) in the tracer-tagged technique (Grewe, 2004). Ideally, this

fraction should be 0% (Grewe, 2004). However, because of the non-linearities of fast ozone photochemistry, there is a deviation. Maximum deviations were on the order of about  $-30\%$  to  $-50\%$  in this study, which is similar to the  $-40\%$  reported by Grewe (2004). To reduce the non-linearities, as suggested by Grewe (2004), the  $C_i^s$  can be scaled following Eq. 3 so that the deviation is 100%:

$$C_i^s = \frac{\sum C_i^t}{\sum C_i^{s'}} C_i^{s'} \quad (3)$$

where  $C_i^{s'}$  is the original estimate in the sensitivity approach, which can be calculated by comparing two simulations, one with and one without emission reductions.  $\sum C_i^{s'}$  is the sum of ozone photochemically produced by all emissions in the model domain. To minimize the impacts of non-linearities of ozone photochemistry and numerical deficiencies, we applied the 50% emission reductions in the sensitivity approach in a manner similar to that of Derwent et al. (2004). In this study, we only took SSD, AH and JS (high ozone production regions) as examples because of the limitations of computing time and resources.

Table 5 presents estimated error ( $E_a$ ) of simulated ozone produced in SSD, AH, and JS in June at Mt. Tai. Case III is excluded because of the negative contributions in sensitivity approach. As suggested by Grewe (2004), the negative contributions should be omitted in the comparison between both approaches. Generally, predicted ozone contributions generated by the tracer-tagged technique agree reasonably well with those of the sensitivity approach. Errors associated with the contributions from SSD mostly were within 7 ppbv

**Table 5.** Estimated errors of contributions from various ozone production regions to ozone mixing ratios at Mt. Tai.<sup>a</sup>

Regions	Monthly mean	Case I	Case II	Case IV
SSD	3.6 (23.5)	7.0 (30.7)	3.3 (13.6)	1.1 (15)
AH+JS	-5.9 (-29.8)	-8.2 (-27.7)	-8.5 (-21.1)	1.0 (30)

<sup>a</sup> Units are ppbv with percentages indicated in brackets.

(30%) during the monthly mean and high ozone events. AH and JS showed similar results (errors of  $\sim 8$  ppbv). This suggests that our results are reasonable. Table 5 also shows overestimates for SSD and underestimates for AH + JS in the tracer-tagged technique except in Case IV; these discrepancies likely were caused by the different treatment by the two techniques of contributions of any given region. The tracer-tagged technique must separate the contributions to local ozone concentrations of regional-scale transport from distinct regions. That is, to track local ozone at Mt. Tai back to regions in which it was produced (Grewe, 2006). What the sensitivity approach reveals is the overall impacts of ozone precursor's emissions themselves from any given region on local ozone at Mt. Tai. As stated by Grewe (2004), this sensitivity approach analyzes the total impacts of an emission source, whereas the tracer-tagged technique assesses the contributions. In this study, the contribution tagged as SSD also included O<sub>3</sub> that was chemically produced over SSD from precursors transported across the border from AH and JS. Consequently, some of the impacts of AH and JS emissions in the sensitivity approach were assigned to be SSD in the tagged technique.

## 5 Exports of near-ground ozone from CEC

Figure 8 presents the spatial distributions of chemically produced ozone in CEC; also shown are contributions from China, NECHN, and ECHN in June 2006. These regions were defined previously in Sect. 2 and Fig. 1. Here, we divide CEC into two parts based on the underlying surface (land and ocean): CEC\* (a high polluting region including HBT, SX, HN, NSD, ESD, Local, SSD, AH, and JS) and CHNSEA (a clean region with no emissions, Fig. 1). In CHNSEA, most of the ozone precursors originated from the transport of CEC\*, so it represents the effect on ozone mixing ratios of the outflow of CEC\* ozone precursors. CEC\* represents the outflow of chemically produced ozone itself in the high polluting region.

Due to the prevailing southerly and southwesterly summer monsoon that occurs over CEC, O<sub>3</sub> formed in CEC\* and CHNSEA is transported toward the northeast to Korea and Japan, where the contribution of transport to monthly mean ozone can reach 5–15 ppbv (Fig. 8b, c). CHNSEA and CEC\* cover similar fractions of the China Sea, Korea Peninsula,

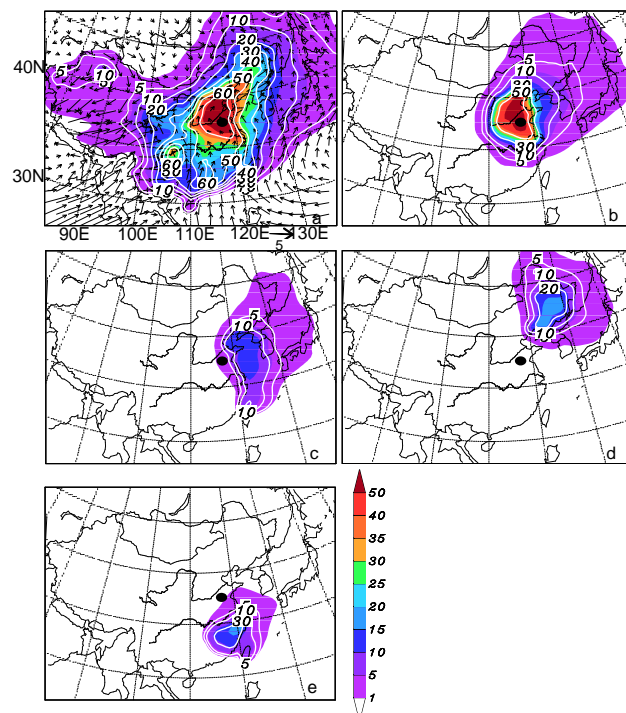


**Fig. 8.** Distributions of contributions (shaded: ppbv; contours: %) from chemically produced ozone over (a) China, (b) CEC\*, (c) CHNSEA, (d) NECHN and (e) ECHN in June 2006. Also shown is wind filed in (a).

and Japan. Thus, in the out flowed ozone, half was due to the direct transport of ozone from CEC and half was contributed by the ozone produced locally by ozone precursors transported from CEC.

Compared with other ozone production regions in China (Fig. 8d, e), CEC is the most important in the export of China's pollutants (Fig. 8a). For example, the ozone export from ECHN is limited to near China's coasts, and the contribution from NECHN is much less than 5% in Japan.

By using back trajectories analysis, Pochanart et al. (2004) estimated the regional photochemical O<sub>3</sub> buildup due to CEC anthropogenic emissions at Oki (36.28° N, 133.18° E, 90 m a.s.l.) and Happo (36.68° N, 137.8° E, 1840 m a.s.l.), two remote sites in Japan, based on 2-year continuous observations in the 1990s. The mean photochemical buildup from CEC in air masses traveling over CEC was about 15–20 ppbv in June. Considering the fraction of air masses traveling over CEC in the total air mass (about 35%), the monthly mean contribution from CEC was 5–7 ppbv, which is similar to the result reported in this study.

## 6 Discussion

Because of the East Asian monsoon system, impacts of regional transport on ozone levels in CEC exhibit significant

seasonal variation. In winter, low temperature suppresses photochemical activity. As a result of the strong prevailing northern winter monsoon, long-range transport from high latitudes (e.g., Siberia) dominates ozone levels in CEC, which is illustrated by the similar ozone concentrations observed at Mondy ( $51^{\circ}39\text{N}$ ,  $100^{\circ}55\text{E}$ , 2006 m a.s.l.) and Mt. Tai (Li, et al., 2007). In spring, with increases in solar radiation and temperatures, cold surges across China frequently blow ozone produced in northern parts (e.g., HBT, SX, NSD) southeastwardly and then out of CEC. The transport from northern regions accounts for a considerable fraction of ozone at Mt. Tai. This is in contrast to the situation in summer observed in this study, where regional-scale transport of ozone photochemically produced in the southern parts (SSD, AH and JS) of CEC was the dominant factor (see Sect. 4). In fall, because of the dominant stable high pressure system in CEC, high ozone was likely produced mostly from local photochemistry. Application of the backward trajectory model to investigate the ozone build up of regional transport revealed a summer maximum – winter-spring minimum pattern (Pochanart et al., 2008). Further quantitative assessment of the seasonal cycle of regional transport from various ozone production regions using the tagged technique will be the subject of a forthcoming paper.

The focus of another future study will be the interannual variability of regional transport, which was discussed by Liu (2003). Because of interannual variations of meteorological fields in CEC, regional transport of ozone exhibits year-to-year variability as well. Chen et al. (2002) reported a strong correlation between the summer monsoon activity in CEC and El Niño/Southern Oscillation (ENSO) in March. In an El Niño year, the southern monsoon in the lower troposphere was focused to the south of  $30^{\circ}\text{N}$ , with an ascending flow in  $25\text{--}30^{\circ}\text{N}$ . In contrast, in a La Niña year the southern meridional flow extended northward to  $50^{\circ}\text{N}$  and the ascending flow moved into CEC ( $32\text{--}37^{\circ}\text{N}$ ), which is clearly a situation more favorable for the transport of ozone produced in the southern parts of CEC to Mt. Tai in June. This scenario is supported by the observations at Mt. Tai, where ozone in a weak La Niña year (this study) had a higher concentration (85 ppbv) than that in a normal year (2004, 78 ppbv). Thus, it would be helpful to develop a long-term simulation with the tagged technique to understand this interannual variability.

## 7 Summary

In this study, we applied the NAQPMS, a 3-D regional chemical transport model with an on-line tracer-tracer-tagged module, to investigate the sources of high ozone levels at Mt. Tai during the MTX2006 project conducted by FR-CGC/JAMSTEC and IAP in June 2006. The influence of various ozone production regions was quantitatively evaluated. The outflows of CEC ozone and its precursors were discussed, and the major findings are summarized as follows:

The performance of the applied regional model was assessed by comparing the simulated results and observations for  $\text{O}_3$ , CO,  $\text{NO}_x$ , and BC. The model was capable of reproducing the temporal variations of the observed ozone and other pollutants over the study period. Except for an underestimation in Case I, the model also captured high polluted and clean cases well.

The simulated tagged tracer technique eliminates the errors caused by non-linearities in the transport and fast photochemistry of ozone and its precursors that are in typical emission sensitivity approach. Our results indicated that the regional transport of ozone chemically produced over other regions of CEC contributed the largest fraction (49%) of near-ground mean ozone at Mt. Tai in June; in situ photochemistry contributed only 12%. Of the transported ozone that was photochemically produced, the contribution from the southern parts in CEC (SSD + AH + JS) played the most important role (32.4 ppbv, 37.9% of total ozone). The contributions from the lateral and top boundaries were 16.4% (14.0 ppbv) and 19.6% (16.7 ppbv), respectively. The error analysis showed a reasonable agreement with the sensitivity approach.

Model simulations of three cases illustrated that the transport of photochemically produced ozone from high anthropogenic sources and biomass burning emissions in the southern parts of CEC (SSD, AH, and JS) played a key role in high ozone events at Mt. Tai. Due to high pressure located over the East China Sea or to the interaction between the Mongolian inverse trough subtropical high pressure, the southern air flows transported high concentrations of ozone from SSD, AH, and JS to Mt. Tai. Their contributions reached 52 ppbv (52%) and 59 ppbv (62%) in Cases I and II, respectively. In contrast, the low amounts of chemically produced ozone from the northern parts of CEC in Case III resulted in the decrease of total ozone at Mt. Tai.

The monthly mean horizontal distributions of chemically produced ozone from various ozone production regions indicated that  $\text{O}_3$  concentrations over CEC were controlled by photochemical production and regional-scale transport, thus these processes played an important role in the distribution of ozone. Chemically produced ozone that came from the south of CEC (SSD + AH + JS) was transported northeastwardly to the northern rim of CEC (a distance of more than 800 km), where the mean contribution was 5–10 ppbv. During high ozone events, this contribution reached 25 ppbv. Ozone produced in the northern parts of CEC was transported out of CEC to northeast China.

The outflows of CEC ozone and its precursors were investigated in the simulation. The contribution from CEC to mean ozone mixing ratios over the Korean Peninsula and Japan was 5–15 ppbv in June. The chemical evolution of ozone precursors during the outflow exerted an effect comparable to that of direct transport of ozone itself from CEC in June.

Finally, these results are helpful to understanding the sources and evolution of high ozone levels in CEC, especially the role of transport. Research to elucidate seasonal cycles and interannual variability is being conducted and will be the subject of a future paper.

*Acknowledgements.* Work of IAP is funded by Chinese Academy of Science (KZCX2-YW-205), the National Basic Research 973 Grant (2005CB422205) and NSFC grant (40775077). This research is sponsored by the RR2002 grant (MEXT, Japan) and the Global Environment Research Fund (B-051 and C-081) of the Ministry of the Environment, Japan). The authors would like to thank all the participants in the MTX2006 field campaign. We also thank Mr. Qizhong Wu for GIS support, R. A. Zaveri for the CBM-Z source code, and Japan Meteorological Agency for O<sub>3</sub> and CO observations at Yonaguni, Japan. We gratefully acknowledge the anonymous reviewers, Yan Zhang at the Princeton University and Gary Morris at Valparaiso University for their helpful comments and suggestions.

Edited by: F. J. Dentener

## References

- Akimoto, H., Kanaya, Y., and Wang, Z.: The Mt. Tai Experiment: June 2006, *Atmos. Chem. Phys. Discuss.*, in preparation, 2008.
- Akimoto, H., Ohara, T., Kurokawa, J., and Horii, N.: Verification of energy consumption in China during 1996–2003 by using satellite observational data, *Atmos. Environ.*, 40, 7663–7667, 2006.
- Brasseur, G., Orland, J. J., and Tyndal, G. S.: *Atmospheric Chemistry and Global Change*, Oxford University Press, New York, 1999.
- Cao, G., Zhang, X., Wang, D., and Zheng, F.: Inventory of atmospheric pollutants discharged from biomass burning in China continent, *China Environmental Science*, 25(4), 389–393, 2005 (in Chinese).
- Chen, Y., Zhou, R., and Jian, J.: The relationship between the summer monsoon circulation in East Asia and ENSO cycle, *Plateau Meteorology*, 21(6), 536–545, 2002 (in Chinese).
- Cheung, V. and Wang, T.: Observational study of ozone pollution at a rural site in the Yangtze Delta of China, *Atmos. Environ.*, 35, 4947–4958, 2001.
- Crutzen, P. J., Lawrence, M. G., and Pöschl, U.: On the background photochemistry of tropospheric ozone, *Tellus* 51A-B, 126–146, 1999.
- Davis, D. D., Chen, G., Grawford, J. H., Liu, S., Tan, D., Sandholm, S. T., Jiang, P., Cunnold, D. M., Dinunno, B., Browell, E. V., Grant, W. B., Fenn, M. A., Anerson, B. E., Barrick, J. D., Sachse, G. W., Vay, S. A., Hudgins, H., Avery, M. A., Lefer, B., Shetter, R. E., Heikes, B. G., Blake, D. R., Kondo, Y., and Oltmans, S.: An assessment of western North Pacific ozone photochemistry based on spring observations from NASA's PEM-West B (1994) and TRACE-P (2001) field studies, *J. Geophys. Res.*, 108(D21), 8829, doi:10.1029/2002JD003-232, 2003.
- Derwent, R. G., Stevenson, D. S., Collins, W. J., and Johnson, C. E.: Intercontinental transport and the origins of the ozone observed at surface sites in Europe, *Atmos. Environ.*, 38, 1891–1901, 2004.
- Ding, A. J., Wang, T., Thouret, V., Cammas, J.-P., and Nédélec, P.: Tropospheric ozone climatology over Beijing: analysis of aircraft data from the MOZAIC program, *Atmos. Chem. Phys.*, 8, 1–13, 2008, <http://www.atmos-chem-phys.net/8/1/2008/>.
- Fu, T. M., Jacob, D. J., Palmer, P. I., Chance, K., Wang, Y. X., Barletta, B., Balke, D. R., Stanton, J. C., and Pilling, M.: Space-based formaldehyde measurements as constraints on volatile organic compound emissions in east and south Asia and implications for ozone, *J. Geophys. Res.*, 112, D06312, doi:10.1029/2006JD007853, 2007.
- Gao, J., Wang, T., Ding, A., and Liu, C.: Observational study of ozone and carbon monoxide at the summit of mount Tai (1534 m a.s.l.) in central-eastern China, *Atmos. Environ.*, 39, 4779–4791, 2005.
- Giglio, L., Descloitres, J., Justice, C. O., and Kaufman, Y. J.: An enhanced contextual fire detection algorithm for MODIS, *Remote Sens. Environ.*, 87(2–3), 273–282, 2003.
- Grell, G. A., Dudhia, J., and Stauffer, D. R.: A description of the Fifth-Generation Penn State/NCAR Mesoscale Model (MM5). Tech. Note NCAR/TN-398+STR, 122 pp., Natl. Cent. For Atmos. Res., Boulder, Colo., 1994.
- Grewe, V.: Technical Note: A diagnostic for ozone contributions of various NO<sub>x</sub> emissions in multi-decadal chemistry-climate model simulations, *Atmos. Chem. Phys.*, 4, 729–736, 2004, <http://www.atmos-chem-phys.net/4/729/2004/>.
- Grewe, V.: The origin of ozone, *Atmos. Chem. Phys.*, 6, 1495–1511, 2006, <http://www.atmos-chem-phys.net/6/1495/2006/>.
- Guenther, A., Hewitt, C. N., Erickson, D., Fall, R., Geron, C., Graedel, T., Harley, P., Klinger, L., Lerdau, M., McKay, W. A., Scholes, B., Steinbrecher, R., Tallamraju, R., Taylor, J., and Zimmerman, P.: A global model of natural volatile organic compound emissions, *J. Geophys. Res.*, 100(D5), 8873–8892, 1995.
- He, Y., Uno, I., Wang, Z., Ohara, T., Sugimoto, N., Shimizu, A., Richter, A., and Burrows, J.: Variations of the increasing trend of tropospheric NO<sub>2</sub> over central east China during the past decade, *Atmos. Environ.* 41, 4865–4876, 2007.
- Intergovernmental Panel on Climate Change (IPCC): *Climate Change 1995*, in: *The Science of Climate Change*, edited by: Houghton, J. T., Ding, Y., Griggs, D. J., Noguer, M., van der Linden, P. J., Dai, X., Maskell, K., and Johnson, C. A., Cambridge Univ. Press, Cambridge, United Kingdom and New York, NY, USA, 1996.
- Kanaya, Y., Pochanart, P., Liu, Y., Tanimoto, H., Kato, S., Suthawaree, J., Inomata, S., Taketani, F., Okuzawa, K., Kawamura, K., Akimoto, H., and Wang, Z.: Rates and regimes of photochemical ozone production over Central East China in June 2006: A box model analysis using comprehensive measurements of ozone precursors, *Atmos. Chem. Phys. Discuss.*, in preparation, 2008.
- Kondo, Y., Nakamura, K., Chen, G., Takegawa, N., Koike, M., Miyazaki, Y., Kita, K., Crawford, J., Ko, M., Blake, D. R., Kawakami, S., Shirai, T., Liley, B., Wang, Y., and Ogawa, T.: Photochemistry of ozone over western Pacific from winter to spring, *J. Geophys. Res.*, 109, D23S02, doi:10.1029/2004JD004871, 2004.
- Li, J., Wang, Z., Akimoto, H., Gao, C., Pochanart, P., and Wang, X.: Modeling study of ozone seasonal cycle in lower troposphere over East Asia, *J. Geophys. Res.*, 112, D22S25,

- doi:10.1029/2006JD008209, 2007.
- Liu, H., Jacob, D., Bey, I., Yantosca, R. M., and Duncan, B.: Transport pathways for Asian pollution outflow over the Pacific: Interannual and seasonal variations, *J. Geophys. Res.*, 108(D20), 8786, doi:10.1029/2002-JD003102, 2003.
- Naja, M. and Akimoto, H.: Contribution of regional pollution and long-range transport to the Asia-Pacific region: Analysis of long-term ozonesonde data over Japan, *J. Geophys. Res.*, 109(D2), D21306, doi:10.1029/2004JD004687, 2004.
- Ohara, T., Akimoto, H., Kurokawa, J., Horii, N., Yamaji, K., Yan, X., and Hayasaka, T.: An Asian emission inventory of anthropogenic emission sources for the period 1980–2020, *Atmos. Chem. Phys.*, 7, 4419–4444, 2007, <http://www.atmos-chem-phys.net/7/4419/2007/>.
- Pochanart, P., Hirokawa, J., Kajii, Y., and Akimoto, H.: Influence of regional-scale anthropogenic activity in northeast Asia on seasonal variations of surface ozone and carbon monoxide observed at Oki, Japan, *J. Geophys. Res.*, 109(D3), 3621–3631, 1999.
- Pochanart, P., Kanaya, Y., Li, J., Komazaki, Y., Akimoto, H., Liu, Y., Wang, X., and Wang, Z.: Surface ozone, carbon monoxide and black carbon over Central East China during MTX2006, *Atmos. Chem. Phys. Discuss.*, in preparation, 2008.
- Pochanart, P., Kato, N., Katsuno, T., and Akimoto, H.: Eurasian continental background and regionally polluted levels of ozone and CO observed in northeast Asia, *Atmos. Environ.*, 38, 1325–1336, 2004.
- Richter, A., Burrows, J. P., N., H., Granier, C., and Niemeier, U.: Increase in tropospheric nitrogen dioxide over China observed from space, *Nature*, 437, 129–132, 2005.
- Streets, D. G., Bond, T. C., Carmichael, G. R., Fernandes, S. D., Fu, Q., He, D., Klimont, Z., Elson, S. M., Tsai, N. Y., Wang, M. Q., Woo, J. H., and Yarber, K. F.: An inventory of gaseous and primary aerosol emissions in Asia in the year 2000, *J. Geophys. Res.*, 108(D21), 8809, doi:10.1029/2002JD003093, 2003.
- Streets, D. G. and Waldhoff, S. T.: Present and future emissions of air pollutants in China: SO<sub>2</sub>, NO<sub>x</sub>, and CO, *Atmos. Environ.*, 34, 363–374, 2000.
- Sudo, K. and Akimoto, H.: Global source attribution of tropospheric ozone: Long-range transport from various ozone production regions, *J. Geophys. Res.*, 112, D12302, doi:10.1029/2006JD007992, 2007.
- Sudo, K., Takahashi, M., Kurokawa, J., and Akimoto, H.: Chaser: a global chemical model of the troposphere. 1. Model description, *J. Geophys. Res.*, 107(D17), 4339, doi:10.1029/2001JD-001113, 2002.
- Tanimoto, H., Wild, O., Kato, S., Furutani, H., Makide, Y., Komazaki, Y., Hashimoto, S., Tanaka, S., and Akimoto, H.: Seasonal cycles of ozone and oxidized nitrogen species in northeast Asia 2. A model analysis of the roles of chemistry and transport, *J. Geophys. Res.*, 107(D23), 4706, doi:10.1029/2001JD001497, 2002.
- van der Werf, G. R., Randerson, J. T., Giglio, L., Collatz, G. J., Kasibhatla, P. S., and Arellano Jr., A. F.: Interannual variability in global biomass burning emissions from 1997 to 2004, *Atmos. Chem. Phys.*, 6, 3423–3441, 2006, <http://www.atmos-chem-phys.net/6/3423/2006/>.
- Waleck, C. J. and Aleksic, N. M.: A simple but accurate mass conservative peak-preserving, mixing ratio bounded advection algorithm with Fortran code, *Atmos. Environ.*, 32, 3863–3880, 1998.
- Wang, T., Ding, A., Gao, J., and Wu, W.: Strong ozone production in urban plumes from Beijing, China, *Geophys. Res. Lett.*, 33, L21806, doi:10.1029/2006-GL027689, 2006a.
- Wang, T., Vincent, T. F., Cheung, M. A., and Li, Y. S.: Ozone and related gaseous pollutants in the boundary layer of eastern China: Overview of the recent measurements at a rural site, *Geophys. Res. Lett.*, 28, 2373–2376, 2001a.
- Wang, Y., Jacob, D., and Logan, J.: Global simulation of tropospheric O<sub>3</sub>-NO<sub>x</sub>-hydrocarbon chemistry 3, Origin of tropospheric ozone and effects of nonmethane hydrocarbons, *J. Geophys. Res.*, 103(D9), 10 757–10 768, 1998.
- Wang, Y., McElroy, M. B., Wang, T., and Palmer, P.: Asian emissions of CO and NO<sub>x</sub> constraints from aircraft and Chinese station data, *J. Geophys. Res.*, 109, D24304, doi:10.1029/2004JD005250, 2004.
- Wang, Z., Akimoto, H., and Uno, I.: Neutralization of soil aerosol and its impact on the distribution of acid rain over East Asia: Observations and model results, *J. Geophys. Res.*, 107(D19), 4389, doi:10.1029/2001JD-001040, 2002.
- Wang, Z., Huang, M., He, D., Xu, H., and Zhou, L.: Sulfur distribution and transport studies in East Asia using Eulerian model, *Adv. Atmos. Sci.*, 13, 399–409, 1996.
- Wang, Z., Li, J., Wang, X., Pochanart, P., and Akimoto, H.: Modeling of regional high ozone episode observed at two mountain sites (Mt. Tai and Huang) in East China, *J. Atmos. Chem.*, 55(3), 253–272, doi:10.1007/s10874-006-9038-6, 2006b.
- Wang Z., Maeda, T., Hayashi, M., Hsiao, L. F., and Liu, K. Y.: A nested air quality prediction modeling system for urban and regional scales, application for high-ozone episode in Taiwan, *Water, Air, and Soil Pollut.*, 130, 391–396, 2001b.
- Wang Z., Ueda, H., and Huang, M.: A deflation module for use in modeling long-range transport of yellow sand over East Asia, *J. Geophys. Res.*, 104, 26 947–26 960, 2000.
- Wesely, M. L.: Parameterization of surface resistances to gaseous dry deposition in regional-scale numerical models, *Atmos. Environ.*, 23, 1293–1304, 1989.
- Xu, X., Lin, W., Wang, T., Yan, P., Tang, J., Meng, Z., and Wang, Y.: Long-term trend of surface ozone at a regional background station in eastern China 1991–2006: enhanced variability, *Atmos. Chem. Phys.*, 8, 2595–2607, 2008, <http://www.atmos-chem-phys.net/8/2595/2008/>.
- Yamaji, K., Ohara, T., Uno, I., Tanimoto, H., Kurokawa, J., and Akimoto, H.: Analysis of the seasonal variation of ozone in the boundary layer in East Asia using the Community Multi-scale Air Quality model: What controls surface ozone levels over Japan?, *Atmos. Environ.*, 40, 1856–1868, 2006.
- Yamaji, K., Li, J., Takigawa, M., Uno, I., Kanaya, Y., Pochanart, P., Liu, Y., Komazaki, Y., Wang, Z., and Akimoto, H.: Evaluating impact of field burning of crop residue on air pollutions for the Mount Tai Experiment 2006 using regional model, *Atmos. Chem. Phys. Discuss.*, in preparation, 2008.
- Zaveri, R. A. and Peters, L. K.: A new lumped structure photochemical mechanism for large-scale applications, *J. Geophys. Res.*, 104, 30 387–30 415, 1999.
- Zhang, M., Uno, I., Carmichael, G. R., Akimoto, H., Wang, Z. F., Tang, Y. H., Woo, J. H., Streets, D. J., Sachse, G. W., Avery, M. A., Weber, R. J., and Talbot, R. W.: Large-scale structure of trace gas and aerosol distributions over the western Pacific Ocean during the Transport and Chemical Evolution Over the Pa-

cific (TRACE-P) experiment, *J. Geophys. Res.*, 108(D21), 8820, doi:10.1029/2002JD002946, 2003.

Zhu, B., Akimoto, H., Wang, Z., Sudo, K., Tang, J., and Uno, I.: Why does surface ozone peak in summertime at Waliguan?, *Geophys. Res. Lett.*, 31, L17104, doi:10.1029/2004GL020609, 2004.